VSP

Journal of Biomaterials Science 22 (2011) 1099–1113

Journal of BIOMATERIALS SCIENCE
brill.nl/jbs

Cross-Linking of Gelatin and Chitosan Complex Nanofibers for Tissue-Engineering Scaffolds

Yong-Fang Qian [a,b], **Kui-Hua Zhang** [b,c], **Feng Chen** [b], **Qin-Fei Ke** [a] **and Xiu-Mei Mo** [b,*]

[a] College of Textiles, Donghua University, Shanghai 201620, P. R. China

[b] Biomaterials and Tissue Engineering Lab, College of Chemistry and Chemical Engineering and Biological Engineering, Donghua University, Shanghai 201620, P. R. China

[c] College of Biological Engineering and Chemical Engineering, Jiaxing College, Jiaxing 314001, P. R. China

Received 8 December 2009; accepted 25 March 2010

Abstract

The aim of this study is to investigate cross-linked gelatin–chitosan nanofibers produced by means of electrospinning. Gelatin and chitosan nanofibers were electrospun and then cross-linked by glutaraldehyde (GTA) vapor at room temperature. Scanning electron microscopy (SEM) images showed that the cross-linked mats could keep their nanofibrous structure after being soaked in deionized water at 37°C. The cross-linking mechanism was discussed based on FT-IR results. The two main mechanisms of cross-linking for chitosan and gelatin–chitosan complex are Schiff base reaction and acetalization reaction. For gelatin, the mechanism of cross-linking was Schiff base reaction. The mechanical properties of nanofibrous mats were improved after cross-linking. The biocompatibility of electrospun nanofibrous mats after cross-linking was investigated by the viability of porcine iliac endothelial cells (PIECs). The morphologies of PIECs on the cross-linked nanofibrous mats were observed by SEM. In addition, proliferation of PIECs was tested with the method of methylthiazol tetrazolium (MTT) assay. The results indicate that gelatin–chitosan nanofibrous mats could be a promising candidate for tissue-engineering scaffolds.

Keywords

Chitosan, gelatin, electrospinning, cross-linking, biocompatibility

1. Introduction

In contrast to conventional transplantation methods, tissue engineering provides new medical therapies using polymeric biomaterials with or without living precursor. The ultimate purpose of tissue engineering is to re-establish destroyed human tissues or organs by providing scaffolds for functional cells regeneration. In human tissues, the extracellular matrix (ECM) plays a pivotal role in supporting and con-

* To whom correspondence should be addressed. E-mail: xmm@dhu.edu.cn

DOI:10.1163/092050610X499447

trolling cells living. Therefore, the tissue-engineering scaffolds should be designed accordingly. The ECM is a complex of structural and functional proteins, glycoproteins and proteoglycans arranged in a unique, tissue-specific 3-D ultrastructure [1]. For mimicking the human ECM which has a nanofibrous structure, electrospun nanofibers have been applied in recent years [2]. Nanofibrous scaffolds fabricated by electrospinning of biomaterials provide suitable environment for cell attachment and proliferation, because of the similar physical dimension compared with natural ECM. Electrospinning is a technique that utilizes electric force alone to drive the spinning process and to produce polymer fibers from solutions or melts [3–5]. Unlike conventional spinning techniques (solution- or melt-spinning), which are capable of producing fibers with diameters in the micrometer range, electrospinning is capable of producing fibers with diameters in the nanometer range. Electrospun polymer nanofibers possess many extraordinary properties, such as small diameters and the concomitant large specific surface areas. Additionally, the non-woven fibrous mats made of electrospun polymer nanofibers offer a unique capability to control the pore sizes among nanofibers. Many synthetic and/or natural polymers including, but not limited to, polylactide (PLA) [6], poly(ε-caprolactone) (PCL) [7], poly(glycolic acid) (PGA) [8], poly(L-lactide-co-ε-caprolactone) (PLACL) [9], proteins [10] and polysaccharides [11] have been electrospun into nanofiber mats as innovative scaffolds for growing various kinds of cells.

Gelatin is one of the most abundant structural proteins found in the animal body (skin, tendon, cartilage and bone), which is obtained by partial hydrolysis of natural collagen by breaking the triple-helix structure of collagen into single-strain molecules. Because of its properties, such as biodegradability, biocompatibility and non-immunogenic, gelatin has been electrospun into nanofibrous type for application in tissue-engineering scaffolds [12–14]. Chitosan is a basic natural polysaccharide derived from chitin, which is the second largest natural resource inferior to cellulose. Because of its abundant production, excellent biocompatibility, appropriate biodegradability, excellent physicochemical properties and commercial availability, it has also been widely used as biomaterials in pharmaceutics, and tissue-engineering and drug-delivery scaffolds. Since gelatin is a protein biopolymer derived from partial hydrolysis of native collagens and chitosan has structural characteristics similar to glycosaminoglycans (GAGs) in the ECM, electrospun gelatin and chitosan complex could mimic the composition and nanofibrous structure of collagen in ECM.

In the present work, gelatin and chitosan complex was successfully electrospun into nanofibers. However, as-electrospun mats without any modification can dissolve water and, thus, cannot keep their structure when used as nanofibrous scaffolds. Therefore, glutaraldehyde (GTA) vapor was used to cross-link the as-spun nanofibrous mats, which is one of the most widely used cross-linking agents in chemical industry because of its high stabilization and effectiveness [15, 16]. The morphologies of the resultant nanofibrous mats were observed by scanning electron microscopy (SEM). Fourier transform infrared spectroscopy (FT-IR) was conducted

to investigate the cross-linking mechanism. The biocompatibility of electrospun nanofibrous mats after cross-linking was investigated by the viability of porcine iliac endothelial cells (PIECs). The morphologies of PIECs on the cross-linked nanofibrous mats were observed by SEM. In addition, proliferation of PIECs was tested with the methylthiazol tetrazolium (MTT) assay.

2. Materials and Methods

2.1. Materials

Chitosan (deacetylation degree approx. 85%. M_η about 10^6) was purchased from Jinan Haidebei Marine Bioengineering. Gelatin (Type A, 300 bloom) was purchased from Sigma-Aldrich.

The solvents used in this work include 1,1,1,3,3,3-hexafluoro-2-propanol (HFP), which was purchased from Daikin Industries, and trifluoroacetic acid (TFA), which was purchased from Shanghai Runjie Chemical Reagent. The cross-linking agent, aqueous GTA (25%), was purchased from Shanghai Chemical Reagent Purchase & Supply Wulian Chemical Plant. All products were used without further purification.

2.2. Electrospinning

Gelatin was dissolved in pure HFP and chitosan was dissolved in HFP/TFA (8:2, v/v), respectively; then, the two solutions were mixed together and HFP/TFA in the final solution was 9:1 (v/v). The concentration of both gelatin and chitosan was 0.08 g/ml. The result solution was fed into a 1 ml plastic syringe. The experimental set-up used for conducting electrospinning included a high voltage power supply (BGG DC high-voltage generator), purchased from BMEI and an extremely accurate syringe pump (789100C, Cole-Parmer). During electrospinning, a positive high voltage of 24 kV was applied at the tip of a syringe needle with the inner diameter of 0.21 mm. The electrospun nanofibers were collected on a piece of aluminum foil (or medical grade plastic cover-slides) covered on an electrically grounded metal plate, which was placed at a distance of 13 cm below the tip of the syringe needle. The mass flow rate was maintained at 0.6 ml/h. Electrospinning was conducted under the ambient conditions. The morphologies of the electrospun nanofibrous mats were observed by SEM and the size distribution were conducted by image visualization software ImageJ 1.34s (NIH).

2.3. GTA Vapor Cross-Linking and Water-Resistance Test

The cross-linking process was carried out by placing the air-dried gelatin and chitosan complex nanofibrous mats supported on aluminum foil in a sealed desiccator containing 10 ml of 25% aqueous GTA solution in a Petri dish. The nanofibrous mats were placed on a holed ceramic shelf in the dessicator and were cross-linked in the GTA vapor for 3 days at room temperature. After cross-linking, the samples were exposed in a fume hood for 2 h followed by circular vacuumization to

remove residual GTA. The cross-linked gelatin and chitosan complex nanofibrous mats were soaked in deioned water at 37°C and resultant mats were dried in a vacuum oven for 1 week, and then observed by SEM (JSM-5600LV) at an accelerating voltage of 10 or 15 kV.

2.4. Fourier Transform Infared Spectroscopy and Nuclear Magnetic Resonance

Raw gelatin and chitosan, casting film, electrospun and cross-linked nanofibrous mats were compressed into slice with KBr power and then analyzed using a FT-IR spectrophotometer (Avatar380). All spectra were recorded by an absorption mode at 2 cm^{-1} intervals in the wavelength range of 4000–500 cm^{-1} wavenumbers.

^{13}C-CP–MAS-NMR spectra were obtained on a NMR spectrometer (Bruker AV 400) with a ^{13}C resonance frequency of 100 MHz, contact time of 1.0 ms and pulse delay time of 4.0 s.

2.5. Mechanical Properties Test

A universal materials tester (H5K-S, Hounsfield) with a load cell of 50 N was utilized to compare the mechanical properties of electrospun and cross-linked chitosan and gelatin complex. Six electrospun and cross-linked mats (30 mm × 10 mm) were tested at ambient temperature (20°C) and humidity of 65%. The specimen thicknesses were measured using a micrometer having a precision of 0.01 mm. A cross-head speed of 10 mm/min was used for all the specimens tested. The machine-recorded data were used to process the tensile stress–strain curves of the specimens.

2.6. PIECs Growth and Morphology on Nanofibers

Porcine iliac endothelial cells (PIECs) were cultured in DMEM medium with 10% fetal serum, 100 U/ml penicillin and 100 U/ml streptomycin in humidified incubator with a 5% CO_2 content at 37°C, and the medium was replaced every 3 days. The coverslips (14 mm in diameter) were put onto the aluminum foil to collect the electrospun nanofiber meshes. Then the meshes were fixed in 24-well plates with a stainless ring and sterilized with 75% alcohol solution, which was replaced with phosphate-buffered saline solution (PBS) after 2 h washing.

PIECs were seeded onto the nanofiber meshes at a density of 3.0×10^4 cells/cm^2 for morphology observed by SEM (S-2700, Hitachi). After 24 h culturing, the cells on the mats were washed with PBS and then fixed with 4% GTA for 45 min at 4°C. Thereafter, the samples were dehydrated in 50, 75 and 100% alcohol solutions, and dried under vacuum. The samples were sputter-coated with gold and observed with SEM at a voltage of 15 kV. For proliferation test, PIECs were seeded onto the nanofiber meshes at a density of 1.5×10^4 cells/cm^2. At 1, 3, 5 and 7 days after cell seeding, unattached cells were washed out and attached cells were quantified using a MTT kit (C0009, Beyotime Institute of Biotechnology) and enzyme-labeled instrument (MK3, Thermo).

3. Results and Discussion

3.1. Fiber Morphologies before and after Cross-Linking

Figure 1 shows SEM micrographs of electrospun mats. The average diameter and size distribution of electrospun nanofibers were 290 ± 154 nm and 144–963 nm for gelatin, 261 ± 119 nm and 108–780 nm for chitosan, and 231 ± 140 nm and 63–707 nm for the gelatin–chitosan complex. The average diameter of the gelatin–

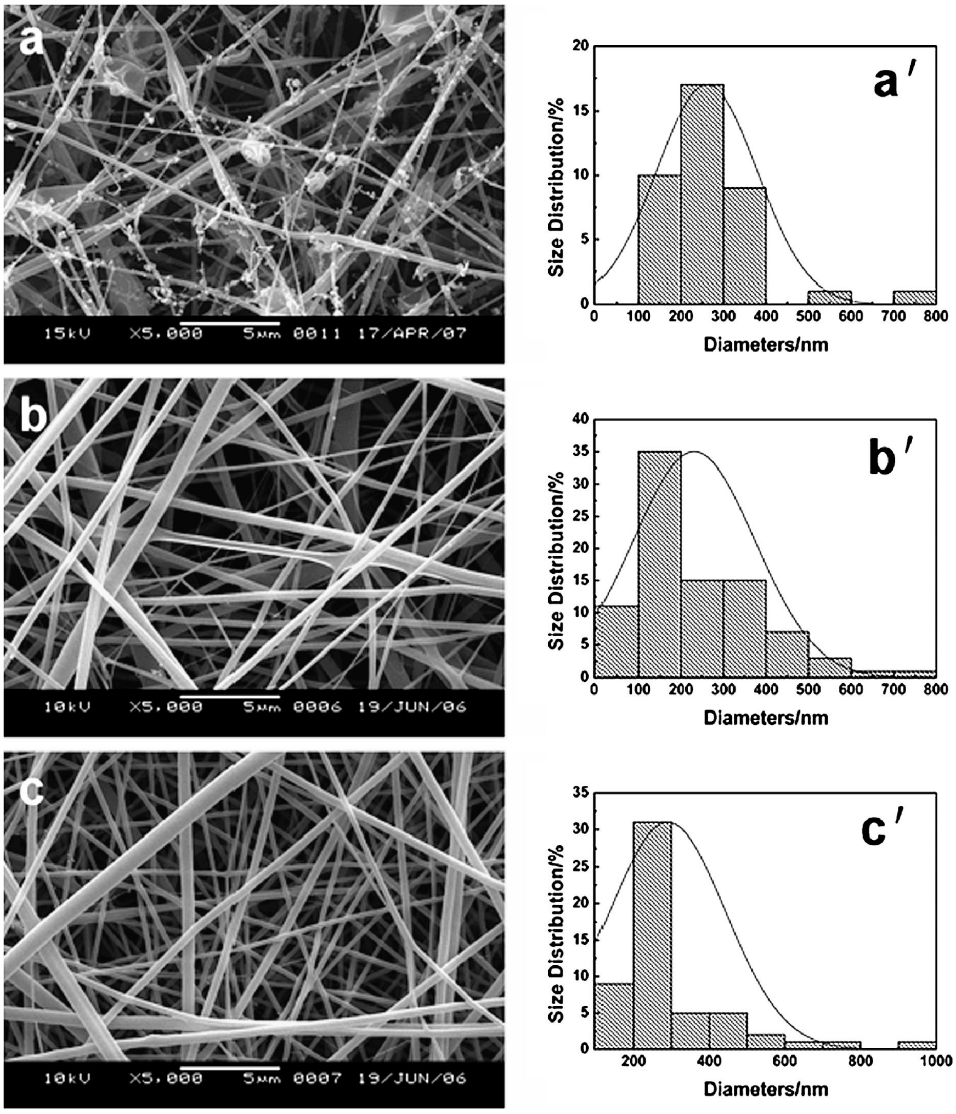

Figure 1. SEM micrographs (a, b, c) and size distribution (a′, b′, c′) of electrospun gelatin and chitosan complex nanofibers. Gelatin/chitosan ratio: (a) 0:100, (b) 50:50 and (c) 100:0.

chitosan complex was slightly lower than that of pure gelatin and pure chitosan. The reason could be the formation of a polyanion–polycation complex between gelatin and chitosan. The addition of ionic salt in the solution could reduce the fiber diameter due to the higher charge density on the surface of the ejected jet and, thus, higher elongation forces applied to the jet [17]. Moreover, the increasing charge density could enhance the jet bending instability and, thus, result in a smaller fiber diameter [18, 19]. Incorporation of gelatin could improve the electrospinability of chitosan, and the resultant nanofibers became smoother.

GTA has been applied to cross-link chitosan [20, 21] and collagen-base materials [22, 23]; however, the conventional cross-linking approach of immersing the samples into aqueous GTA solution is not feasible for cross-linking the present gelatin–chitosan nanofibrous mats because of the high solubility in water. By placing the nanofibers into a desiccator filled with GTA vapor, the gelatin–chitosan nanofibers can be cross-linked reasonably. Figure 2 shows the fiber morphologies of the samples after cross-linking and water resistant test. Samples a-crs, b-crs and c-crs are the gelatin and chitosan fibers before the water-resistance test, and samples a-soa, b-soa and c-soa are the gelatin and chitosan fibers dried in a vacuum oven for 1 week after being soaked in DI water for 4 days at 37°C. The co-existence of water moisture with GTA vapor during cross-linking treatment has affected the fiber morphologies to some extent. The electrospun mats could keep their nanofibrous structure after cross-linking. For the water-resistance test, the nanofibrous structure was preserved, even after being soaked for 4 days at 37°C. The results indicated that GTA is an effective cross-linking agent to treat gelatin and chitosan.

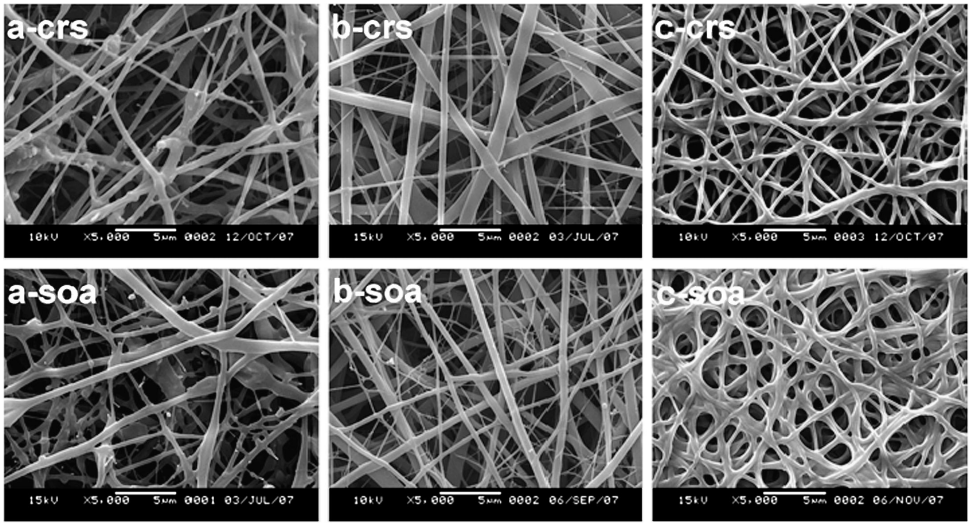

Figure 2. SEM micrographs of cross-linked (-crs) and soaked (-soa) mats of (a) chitosan, (b) cross-linked gelatin–chitosan complex (50:50) and (c) gelatin.

3.2. FT-IR Analysis of Electrospun and Cross-Linked Gelatin and Chitosan Complex

3.2.1. Effect of Solvents on Gelatin and Chitosan

Figure 3 shows the FT-IR spectra of raw chitosan and its cast film from HFP/TFA in whole range and in large size. The FT-IR spectrum of chitosan shows characteristic absorption peaks at 3442, 1650, 1600, 1380, 1320, 1260, 1157, 1083 and 898 cm^{-1}. The amino group ($–NH_2$) has a characteristic absorption band in the region of 3400–3500 cm^{-1}. The hydroxy group (–OH) has absorption peaks at 3200–3400 cm^{-1}; therefore, the broad absorption peak at 3442 cm^{-1} is attributed to the amino group ($–NH_2$) stretching vibration and –OH stretching vibration. Peaks at 1157 and 898 cm^{-1} represent the saccharide structure of chitosan. The characteristic peak at 1650 cm^{-1} represents the amide I absorption band, and those at 1320 and 1260 cm^{-1} represent the amide III absorption band corresponding to C=O stretching vibration and C–N stretching vibration, respectively. Amide I and amide III absorption bands suggest that chitosan is a partially deacetylated product. The spectrum of the chitosan cast membrane in large size is shown in Fig. 3b. The peak of 1790 cm^{-1} was due to the presence of CO–F. However, the CO–F group was not stable, and it turned into carboxylic acid after cross-linking due to hydrolysis. The absorption peak at 1540 cm^{-1} represents the amide II band, and this arises from the coupling of N–H bending vibration and C–N stretching vibration. Three new absorption peaks appeared in the region of 840–720 cm^{-1}. The results indicate that chitosan reacted with TFA and formed amine salts [24, 25]. The electrospun solvents were mixtures of HFP and TFA. HFP is widely used in dissolving proteins and polysaccharides, because it is a strong polar solvent. TFA was added into the solution to improve dissolving ability because TFA forms salts with the amino groups and this salt formation destroys the rigid interaction [26]. The process that TFA dissolves chitosan and then forms amine salt is composed of two stages: the free amino in molecular is first protonized and then $–NH_3^+$ forms amine salts with the anion in TFA. This process is shown in Fig. 4.

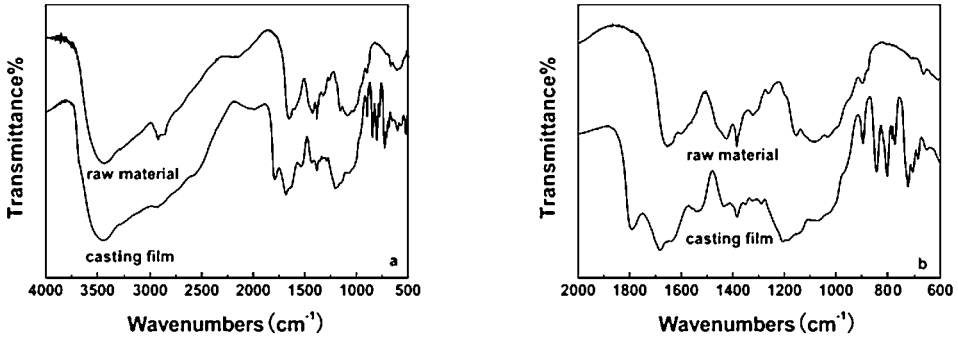

Figure 3. FT-IR spectra of chitosan raw material and casting film. (a) Whole range and (b) in large size.

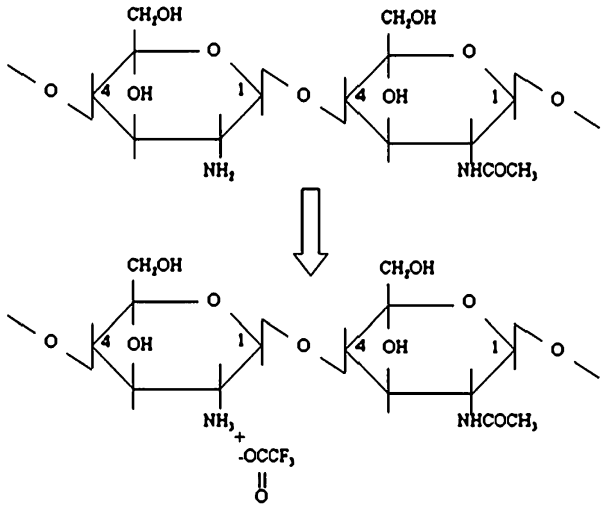

Figure 4. Chemical structure changes after dissolving in TFA.

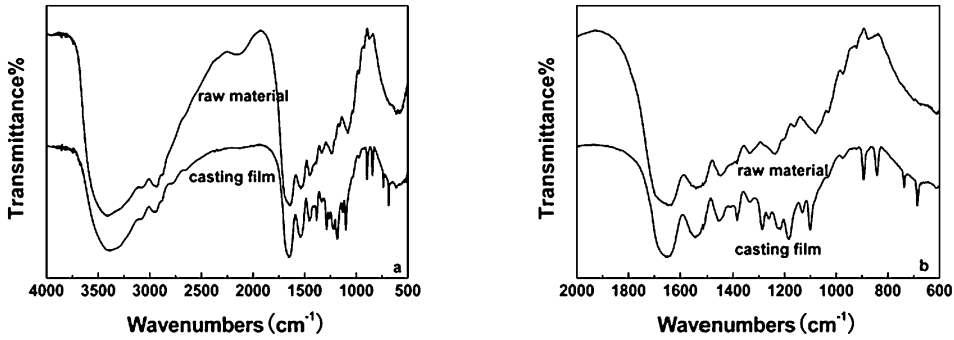

Figure 5. FT-IR spectra of gelatin raw material and casting film. (a) Whole range and (b) in large size.

Gelatin displays absorption peaks at 1645, 1535 and 1240 cm^{-1}, which represent amide I, amide II and amide III characteristic absorption bands, as shown in Fig. 5. The amide I band arises predominantly from protein amide C=O stretching vibration. The amide II absorption is made up of N–H bending vibration and C–N stretching vibrations. The amide III peak is caused by C–N stretching vibration. After dissolving, the spectrum has new absorption in the region 840–720 cm^{-1} implying that amine salts were also formed.

3.2.2. FT-IR Spectra of Electrospun Gelatin and Chitosan Complex

Figure 6 shows the FT-IR spectra of electrospun gelatin, chitosan, and their blend (50:50). Compared with raw chitosan and dissolved chitosan, electrospun chitosan has an absorption peak at 1680 cm^{-1} which represents the amide I characteristic band. The absorption peak at 1260 cm^{-1} (amide III) disappeared after electrospinning. The spectrum of electrospun gelatin was similar to those of gelatin and

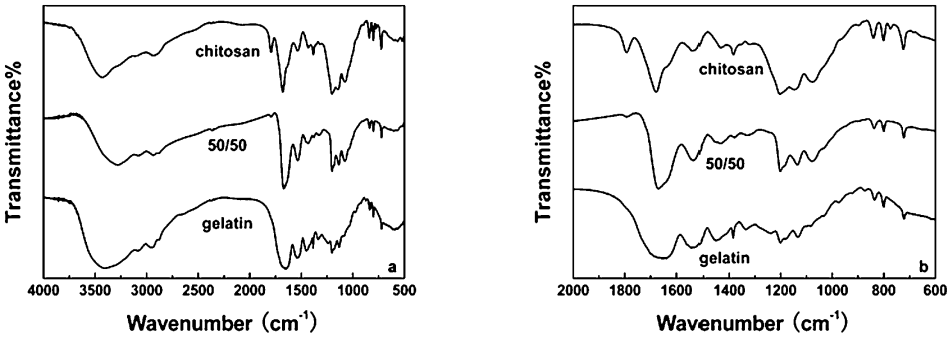

Figure 6. FT-IR spectra of electrospun gelatin, chitosan and their complex nanofibrous mats. (a) Whole range and (b) in large size.

dissolved gelatin. The position of absorption peaks shifted in the region of 3200–3500 cm^{-1} and in the amide I absorption band. Electrospun gelatin, chitosan and their complex (50:50, w/w) show characteristic peaks at 3396, 3428 (electrospun gelatin), 3280 (gelatin) and 1650, 1680 and 1670 cm^{-1} (complex), respectively. Therefore, the shift of both carbonyl and amino bands in the spectra of electrospun chitosan–gelatin complex provided evidence that chitosan and gelatin formed a hydrogen bonding [27, 28]. The –OH groups, $–NH_2$ groups and the –C=O groups in gelatin are capable of forming hydrogen bonds with –OH and $–NH_2$ groups in chitosan. Additionally, ionic bonds maybe formed between gelatin and chitosan. These molecules are capable of forming a complex with oppositely charged ionic polymers, especially the cationic polysaccharide chitosan and anionic –COOH group in gelatin. These interactions may form a polyanionic–polycationic complex [29].

3.2.3. FT-IR Spectra of Cross-Linked Gelatin and Chitosan Complex

As a result of the cross-linking reaction, nanofibrous mats became yellow after cross-linking while the as-spun nanofibrous mats were white. Also, cross-linked chitosan turned into dark yellow, cross-linked gelatin turning into light yellow, and their complex in the medium. Figure 7 shows the FT-IR spectrum of electrospun and GTA-cross-linked chitosan. The FT-IR spectrum of GTA-cross-linked chitosan has a strong absorption at 1680 cm^{-1}. Since the absorption peak of imine –C=N– stretching vibration could be in the range of 1640–1690 cm^{-1}, overlapping with the strong absorption of the amide I band in chitosan. Besides, the spectrum had four absorption peaks in the region of 1000–1200 cm^{-1} and a new absorption peak at 1030 cm^{-1} appeared after cross-linking. These could be attributed to the acetalyzation reaction between hydroxyl groups (–OH) in chitosan and carbonyl (=CO) in GTA and the formed C–O–C–O–C structure.

Figure 8 shows the FT-IR spectrum of electrospun and GTA-cross-linked gelatin. The spectrum of cross-linked gelatin has a strong absorption at 1650 cm^{-1} which is also overlapped by the absorption of the amide I band in gelatin. The absorption peak of free $–NH_2$ groups and –OH groups in gelatin shifted from 3396 to

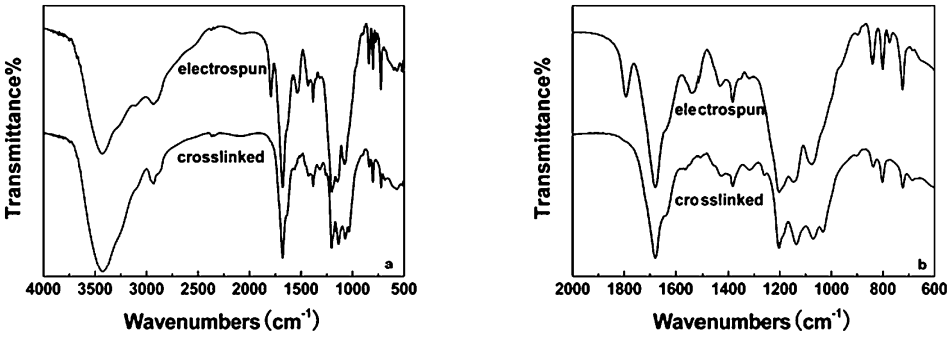

Figure 7. FT-IR spectra of electrospun and cross-linked chitosan. (a) Whole range and (b) in large size.

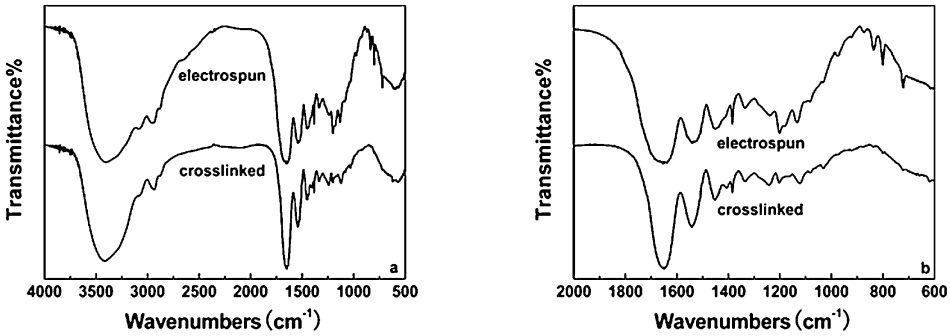

Figure 8. FT-IR spectra of electrospun and cross-linked gelatin. (a) Whole range and (b) in large size.

3415 cm^{-1}. Schiff base (–C=N) was formed by free amino groups in lysine and arginine of gelatin reacting with the aldehyde groups of glutaraldhyde.

In the spectrum of the cross-linked chitosan–gelatin complex, the absorption peak of the free amino group and OH group shifted from 3278 to 3420 cm^{-1}, as shown in Fig. 9. Moreover, the spectrum had four absorption peaks in the region 1000–1200 cm^{-1} since a new absorption peak at 1030 cm^{-1} exists after cross-linking, similar to chitosan. The C–O–C–O–C structure was formed after cross-linking.

Combining the color change with FT-IR analysis, the results imply that chitosan has a higher reaction tendency to be cross-linked with GTA, as compared with its gelatin counterpart. Two main mechanisms of cross-linking for chitosan were Schiff base reaction that formed imine structure (–C=N) and acetalization reaction that formed C–O–C–O–C structure. The mechanism of cross-linking for gelatin was a Schiff base reaction. For the chitosan–gelatin complex, the mechanisms were similar to that of chitosan, involving Schiff base reaction and acetalyzation reaction.

The ^{13}C-NMR spectra of electrospun gelatin, chitosan and their complex are shown in Fig. 10a. The spectrum of the complex was the combination of gelatin and chitosan. After being cross-linked and soaked in water, the spectrum of the complex

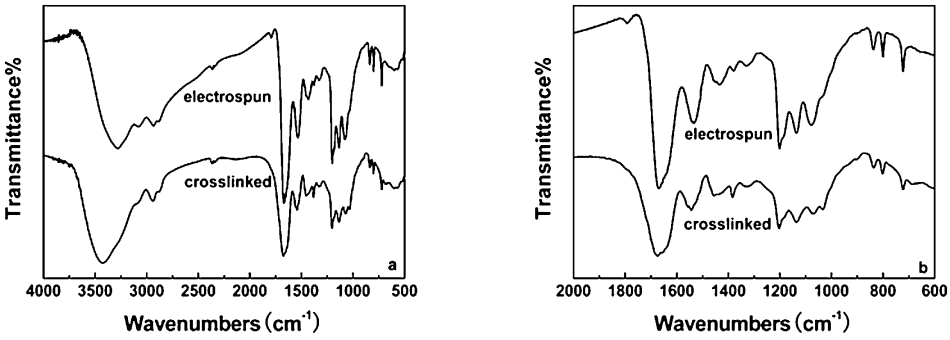

Figure 9. FT-IR spectra of electrospun and cross-linked gelatin–chitosan complex (50:50). (a) Whole range and (b) in large size.

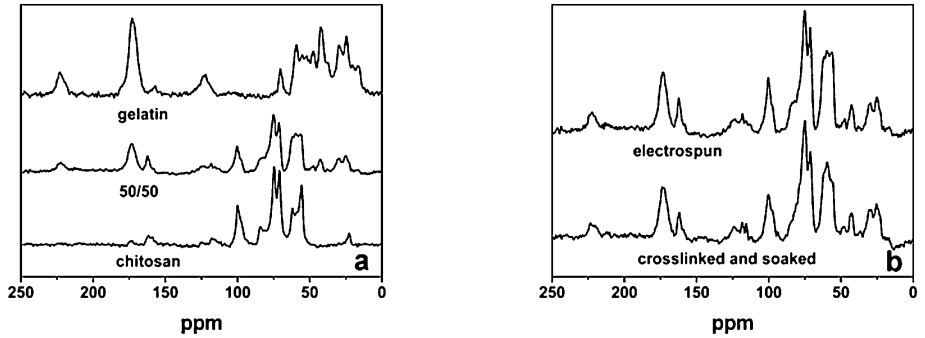

Figure 10. ^{13}C-CP/MAS-NMR spectra of (a) electrospun gelatin, chitosan and their complex and (b) the cross-linked and soaked complex.

was similar to that of electrospun nanofibers, as shown in Fig. 10b, implying the co-existence of chitosan and gelatin after immersion in water.

3.3. Mechanical Properties of Electrospun and Cross-Linked Chitosan–Gelatin Complex

Table 1 lists the average tensile strengths and elongation of electrospun gelatin, chitosan and their blend nanofibrous mats. Electrospun gelatin mats have the largest tensile strength and tensile elongation, and electrospun chitosan mats have the lowest. After cross-linking, the tensile strength of the samples improved to different extents. Formation of point-bonded structures favors the structural integrity of electrospun fibers and, hence, results in improved mechanical properties. The failure process of nanofibrous mats involved slippage and break of fibers. After cross-linking, fibers were bonded with each other, which could avoid slippage. Therefore, the tensile strength was dramatically improved. From SEM morphology, cross-linked gelatin had more fiber-bonded points, as a result, the average tensile strength is larger than that of chitosan, as well as that of the gelatin–chitosan complex. Both

Table 1.
Tensile properties of electrospun and cross-linked gelatin–chitosan nanofibrous mats ($n = 3$)

Gelatin/Chitosan	Average tensile elongation (%)	Average tensile strength (MPa)	Average thickness (μm)
100:0			
Before cross-linking	3.10 ± 0.31	3.54 ± 0.15	91.3 ± 3.5
After cross-linking	1.87 ± 0.08	9.22 ± 1.21	32 ± 2.6
50:50			
Before cross-linking	2.71 ± 0.16	2.07 ± 0.18	105.7 ± 5.4
After cross-linking	2.30 ± 0.42	8.04 ± 0.39	40 ± 2.6
0:100			
Before cross-linking	1.72 ± 0.17	1.93 ± 0.21	84.3 ± 5.4
After cross-linking	1.31 ± 0.18	2.62 ± 0.08	34 ± 4

Thicknesses were measured using a micrometer with a precision of 0.01 mm.

electrospun and cross-linked gelatin–chitosan mats showed brittle mechanical behavior.

3.4. PIECs Growth and Morphology on Gelatin/Chitosan Nanofibrous Mats

The biocompatibility of cross-linked gelatin and chitosan nanofibrous mats was evaluated *in vitro* by observing and testing the behavior of PIECs cultured on the nanofibrous mats. Figure 11 shows the SEM micrographs of cells' morphology on cross-linked gelatin and chitosan complex after 24 h culturing. It can be seen that PIECs spread well on the surface of gelatin, chitosan and complex nanofibrous mats and cells interact and integrate well with the surrounding fibers. Cells on the surface of gelatin nanofibers have a shuttle-like shape, while cells on the surface of complex and chitosan nanofibers have a polygonal shape, indicating that incorporation of chitosan is beneficial to differentiation of cells. Moreover, cells on gelatin–chitosan complex nanofibers could migrate into the meshes through the pore. The cross-linked gelatin and chitosan nanofibrous mats could maintain their fibrous structure well in medium. Thus, they could provide steady physical and chemical support for cell growth.

Proliferation of PIECs on gelatin–chitosan complex nanofibrous mats was tested with the method of MTT assay on the days 1, 3, 5 and 7 after seeding, as shown in Fig. 12. The cell numbers on cross-linked nanofibers after 1 day are less than that of TCPs. From the day 1 to the day 3, cells on cross-linked gelatin and complex proliferated faster than that on cross-linked chitosan. From day 5 to day 7, cells on gelatin and chitosan complex keep proliferate steadily and do not have a significant difference among the three ratios. Gelatin and chitosan complex nanofibers have components and structure similar to that of native ECM. Cells exhibit an ascending trend on cross-linked gelatin and chitosan nanofibrous mats during the 7 days, implying the low cytotoxicity of GTA vapor cross-linking. However, residual

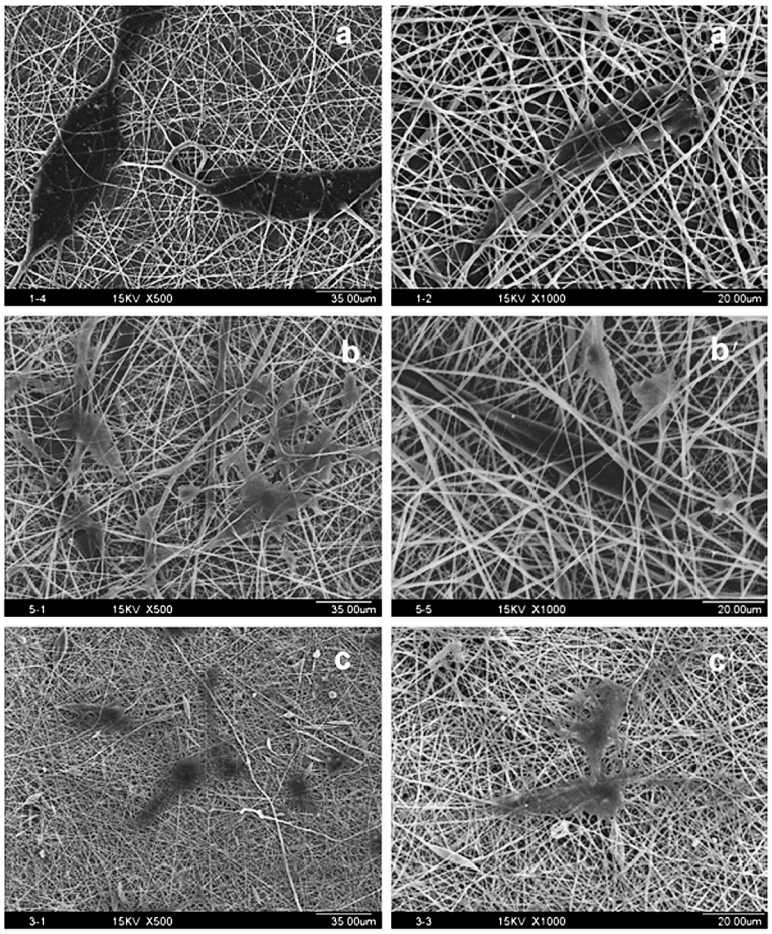

Figure 11. Morphology of PIECs on gelatin–chitosan complex and gelatin/chitosan. (a, a′) 100:0, (b, b′) 50:50 and (c, c′) 0:100. Magnification: (a, b, c) ×500, (a′, b′, c′) ×1000.

GTA molecules might exist in the cross-linked nanofibrous mats. Therefore, it is recommendable to treat the nanofibrous mats with glycine to block unreacted aldehyde group of GTA for better cell proliferation. On day 7, the number of cells on TCPs and coverslips was clearly reduced, as shown in Fig. 12. The reduction of cell number on TCPs and coverslips between days 5 and 7 may be caused by excessive proliferation of PIECs. It may lead to the lack of nutrition. Thereafter, many cells died and were washed out by PBS solution before the MTT test.

4. Conclusion

Gelatin and chitosan complex nanofibrous scaffolds were obtained by electrospinning to mimic natural ECM. Incorporation of gelatin could improve the electrospinability of chitosan, and the electrospun nanofibers became smoother. GTA is

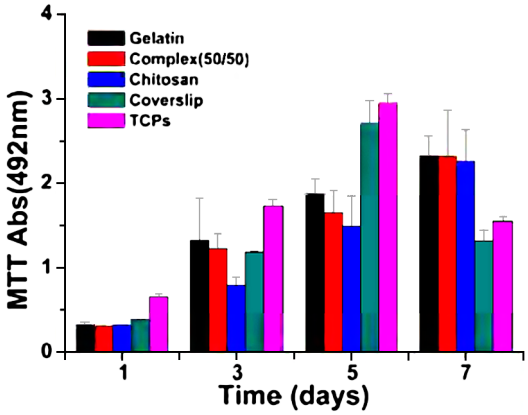

Figure 12. Proliferation of PIECs on gelatin and chitosan nanofibrous mats, coverslips and TCPs. This figure is published in colour in the online edition of this journal, that can be accessed *via* http://www.brill.nl/jbs

an effective cross-linking agent to treat gelatin and chitosan complex. After cross-linking, the as-electrospun matrix can preserve nanofibrous morphologies after being soaked for 4 days. The cross-linking mechanism was examined by FT-IR analysis. For chitosan and the gelatin–chitosan complex, the two main mechanisms were Schiff base reaction and acetalyzation, while the mechanism of cross-linking was Schiff base reaction for gelatin. The mechanical properties of electrospun and cross-linked nanofibrous mats were studied. It was found that mechanical properties were improved after cross-linking. Cell behavior on nanofibrous scaffolds was investigated by SEM and MTT test. Although significant difference was not observed for gelatin, chitosan and their complex, endothelial cells proliferated well on the nanofiber. The results indicate that gelatin–chitosan nanofibrous mats could be a promising candidate for tissue-engineering scaffolds.

Acknowledgements

This research was supported by the National Science Foundation (30570503), National High Technology Research and Development Program (863 Program, 2008AA03Z305) and the "111 Project" Biomedical Textile Materials Science And Technology (B07024).

References

1. S. F. Bidylak, *Semin. Cell. Dev. Biol.* **13**, 377 (2002).
2. B. M. Min, Y. You, J. M. Kim, S. J. Lee and W. H. Park, *Carbohydr. Polym.* **57**, 285 (2004).
3. A. Aluigi, A. Varesano, A. Montarsolo, C. Vineis, F. Ferrero, G. Mazzuchetti and C. Tonin, *J. Appl. Polym. Sci.* **104**, 863 (2007).
4. L. M. Bellan and H. G. Craighead, *J. Vac. Sci. Technol. B* **24**, 3179 (2006).
5. A. Alli, B. Hazer, Y. Menceloglu and E. Suzer, *Eur. Polym. J.* **42**, 740 (2006).

6. J. B. Chiu, C. Liu, B. S. Hsiao, B. Chu and M. Hadjiargyrou, *J. Biomed. Mater. Res. A* **83**, 1117 (2007).
7. N. Bolgen, I. Vargel, P. Korkusuz, Y. Z. Menceloglu and E. Piskin, *J. Biomed. Mater. Res. B* **81**, 530 (2007).
8. L. I. Ramdhanie, S. R. Aubuchon, E. D. Boland, D. C. Knapp, C. P. Barnes, D. G. Simpson, G. E. Wnek and G. L. Bowlin, *Polym. J.* **38**, 1137 (2006).
9. X. M. Mo, C. Y. Xu, M. Kotaki and S. Ramakrishna, *Biomaterials* **25**, 1883 (2004).
10. W. Li, Y. Guo, H. Wang, D. Shi, C. Liang, Z. Ye, F. Qing and J. Gong, *J. Mater. Sci. Mater. Med.* **19**, 847 (2008).
11. S. De Vrieze, P. Westbroek, T. Van Camp and L. Van Langenhove, *J. Mater. Sci.* **42**, 8029 (2007).
12. Z. M. Huang, Y. Z. Zhang, S. Ramakrishna and C. T. Lim, *Polymer* **45**, 5361 (2004).
13. M. Y. Li, J. Mondrinos, M. R. Gandhi, F. K. Ko, A. S. Weiss and P. I. Lelkes, *Biomaterials* **26**, 5999 (2005).
14. S. A. Sell, M. J. McClure, K. Garg, P. S. Wolfe and G. L. Bowlin, *Adv. Drug Deliv. Rev.* **61**, 1007 (2009).
15. K. Tomihata and Y. J. Ikada, *J. Polym. Sci. Pol. Chem.* **35**, 3553 (1997).
16. J. Z. Knaul, S. M. Hudson and K. A. M. Creber, *J. Polym. Sci. Polym. Phys.* **37**, 1079 (1999).
17. X. Zong, K. Kim, D. Fang, S. Ran, B. S. Hsiao and B. Chu, *Polymer* **43**, 4403 (2002).
18. J. S. Choi, S. W. Lee, L. Jeong, S. Bae, B. C. Min, J. H. Youk and W. H. Park, *Int. J. Biol. Macromol.* **34**, 249 (2004).
19. T. Subbiah, G. S. Bhat, R. W. Tock, S. Parameswaran and S. S. Ramkumar, *J. Appl. Polym. Sci.* **96**, 557 (2005).
20. S. R. Jameela and A. Jayakrishnan, *Biomaterials* **16**, 769 (1995).
21. C. Tual, E. Espuche, M. Escoubes and A. Domard, *J. Polym. Sci. Polym. Phys.* **38**, 1521 (2000).
22. L. H. H. Olde Damink, P. J. Dijkstra, M. J. A. van Luyn, P. B. van Wachem, P. Nieuwenhuis and J. Feijen, *J. Mater. Sci. Mater. Med.* **6**, 460 (1995).
23. L. Marincucci, C. Lilli, M. Guerra, S. Belcastro, E. Becchetti, G. Stabellini, E. M. Calvi and P. Locci, *J. Biomed. Mater. Res. A* **67**, 504 (2003).
24. M. Hasegwa, A. Isogai, F. Onabe and M. Usuda, *J. Appl. Polym. Sci.* **45**, 1857 (1992).
25. P. Sangsanoh and P. Supaphol, *Biomacromolecules* **7**, 2710 (2006).
26. K. Ohkawa, D. Cha, H. Kim, A. Nishida and H. Yamamoto, *Macromol. Rapid Commun.* **25**, 1600 (2004).
27. M. N. Taravel and A. Domard, *Biomaterials* **14**, 930 (1993).
28. M. Cheng, J. Deng, F. Yang, Y. Gong, N. Zhao and X. Zhang, *Biomaterials* **24**, 2871 (2003).
29. Y. J. Yin, K. D. Yao, G. X. Cheng and J. B. Ma, *Polym. Int.* **48**, 429 (1999).